Applied Thermal Engineering 230 (2023) 120656

Contents lists available at ScienceDirect

Applied Thermal Engineering

journal homepage: www.elsevier.com/locate/apthermeng

Research Paper

Thermo-economic assessment and optimization of a multigeneration system powered by geothermal and solar energy

Mahmoud Mohammadi [a], Alireza Mahmoudan [a], Pedram Nojedehi [b], Siamak Hoseinzadeh [c,*], Mani Fathali [a], Davide Astiaso Garcia [c]

[a] Department of Aerospace Engineering, K.N. Toosi University of Technology, Tehran, Iran
[b] Department of Civil and Environmental Engineering, Carleton University, Ottawa, ON, Canada
[c] Department of Planning, Design, and Technology of Architecture, Sapienza University of Rome, Via Flaminia 72, Rome 00196, Rome, Italy

ARTICLE INFO

Keywords:
Solar energy
Geothermal energy
Solar tower
Desalination
Multigeneration system
Multi-objective optimization

ABSTRACT

A novel multigeneration system using dual renewable energy sources (i.e., geothermal and solar) is introduced, analyzed, and optimized. The integration of a geothermal line, a solar tower, a steam Rankine cycle, two organic Rankine cycles, an ejector refrigeration cycle, a thermoelectric generator unit, and a reverse osmosis subsystem forms the entire system. The outputs of this energy-conversion system are heating load, cooling load, electricity, and freshwater. Regarding methodology, the energy, exergy, and exergoeconomic approaches are implemented to assess the system from thermodynamic and economic viewpoints. Moreover, an optimization process based on exergy efficiency and the total unit cost of products is executed to determine the system's optimal decision variables. The results obtained from the optimization process show that the proposed system is able to achieve 25.4% exergy efficiency and 34.1 $/GJ total unit cost of products, exhibiting 48% and 43% improvement compared to a base case study. Furthermore, the methodology is demonstrated on a case study where the system operates at its optimum condition in a specific location. Having monthly average values of direct normal irradiation for this spot, the average hourly performance of the system is evaluated for each month. Based on the obtained results, the minimum and maximum freshwater production rates are 3.06 kg/s and 3.84 kg/s, respectively. It can be estimated that a range of 1224 to 1536 individuals, varying from month to month, can receive the produced freshwater.

1. Introduction

The climate risks such as the global warming crisis have become increasingly a pressing problem facing people and societies worldwide. According to the new IPCC report, it demands serious actions and fundamental changes to enhance our ability to deal with climate change [1]. Energy production is a major contributing factor to this issue [2]. This clearly highlights the necessity of harnessing environmentally-benign energy resources that are the backbone of the transition to sustainable and green energy systems. Some renewable energies are obtainable and abundant in nature, such as solar, biomass, wind, waves, tides, hydro, ocean currents, ocean thermal, and geothermal [3,4]. Despite the fact that renewable energy resources significantly reduce the adverse impacts on the environment, their conversion efficiency, like any other processes, is still limited due to irreversibilities. To this end, multi-generation processes are a promising solution. Generating multi-products/outputs from the same energy resource is an avenue to expand resource utilization [5]. A multi-generation system can produce electricity, heating, cooling, hot water, fresh water and hydrogen. Therefore, deploying multi-generation energy systems driven by renewable energy resources must be prioritized over fossil fuel and even renewable energy systems having only a single product such as electricity.

Among the aforementioned renewable energy sources, solar and geothermal possess the potential to sufficiently fulfill multiple needs, such as the energy demands of societies. According to the WEA (world energy assessment) report, geothermal energy has the largest resources compared with solar photovoltaics, wind and hydro energies in the world [6,7]. The overall efficiency of geothermally-driven power conversion systems is higher than for the majority of other forms of energy. Furthermore, geothermal power plants are known for their higher capacity factors (typically over 90%). As a result, they generally are operated 24/7, producing plentiful amounts of baseload power and heat

* Corresponding author.
E-mail addresses: siamak.hosseinzadeh@uniroma1.it, Hoseinzadeh.siamak@gmail.com (S. Hoseinzadeh).

https://doi.org/10.1016/j.applthermaleng.2023.120656
Received 16 October 2022; Received in revised form 5 March 2023; Accepted 25 April 2023
Available online 2 May 2023

Nomenclature

A	Surface area (m^2)
c	Cost per exergy unit ($/GJ)
$\dot{C}$	Cost rate ($/h)
C	Cost ($)
CRF	Capital recovery factor (–)
DNI	Direct normal irradiation (W/m^2)
$\dot{E}x$	Exergy rate (kW)
ex	Specific exergy (kW/kg)
FF	Fouling factor (–)
h	Specific enthalpy (kJ/kg)
i	Interest rate (–)
k_w	Membrane water permeability (–)
$LMTD$	Log mean temperature difference (K)
M	Volumetric flow rate (m^3/h)
$\dot{m}$	Mass flow rate (kg/s)
n	Number (–)
N	Overall operating time of system (h)
P	Pressure (kPa)
PR	Pressure ratio (–)
$\dot{Q}$	Heat transfer rate (kW)
R	Universal gas constant (J/mol-K)
RR	Recovery ratio (–)
s	Specific entropy (kJ/kg-K)
SR	Salt rejection (%)
T	Temperature (°C)
V	Velocity (m/s)
X	Salt concentration (–)
ZT	Figure of merit
TCF	Temperature correction factor (–)
U	Heat transfer coefficient (kW/m^2-K)
$\dot{W}$	Power (kW)
Z	Capital cost ($)
$\dot{Z}$	Investment cost rate ($/h)

Subscripts

0	Dead state condition
ac	Actual
amb	Ambient
av	Average
b	Brine
c	Cold
carnot	Carnot
ch	Chemical
Comp	Compressor
Cooling	Cooling
D	Destruction
d	Diffuser
e	Element
eje	Ejector
en	Energy
exe	Exergy
exp	Expansion valve
Eva	Evaporator
f	Feed
fw	Freshwater
Geo/geo	Geothermal
h	Hot
hel	Heliostat
HP	High Pressure
HRank	High Pressure Rankine
HX	Heat Exchanger
i	Inlet
is	Isentropic
j	Random number associated with streams
k	Random number associated with components
m	Mixing, Mean
n	Nozzle
net	Net
o	Outlet
opt	Optical
P	Product
pv	Pressure vessel
pump	Pump
Q	Heat transfer
rec	Receiver
R	Rankine
s	Secondary
sol	Solar
solar	Solar
tot	Total
tur	Turbine
T	Turbine
w	Water

Greek

η	Efficiency (%)
ρ	Density (kg/m^3)
μ	Entrainment ratio
Δ	Difference

Abbreviation

CRF	Capital recovery factor
DNI	Direct normal irradiation
ERC	Ejector refrigeration cycle
HPP	High pressure pump
HX	Heat exchanger
ORC	Organic Rankine cycle
PTC	Parabolic trough collector
RO	Reverse osmosis
SRC	Steam Rankine cycle
TCF	Temperature correction factor

[8,9]. However, the recent growth in wind and solar deployment presents an opportunity to increase the value of geothermal generation through flexible operations [10]. Similarly, appropriate technologies for harvesting and supplying solar energy are adopted. In that case, the energy demands of the entire world will be theoretically met by solar energy alone. Reducing fossil fuel consumption is one of the key benefits of installing solar thermal systems: a 1–2% reduction has been reported. This type of green energy is also a suitable replacement for scarce renewable sources used in energy systems, such as biomass, and projected to be increasingly demanded in the transport and industrial sectors [11].

A number of papers have been dedicated to the assessment of multigeneration systems supported by geothermal energy. As for methodology, energy, exergy, and exergoeconomic (3E) analyses are applied for technical and economic evaluations [12–16]. Furthermore, a few papers have incorporated a desalination unit into their multigeneration systems driven by geothermal energy. Mahmoudan et al. [17] examined a polygeneration system for heating, cooling, electricity, and freshwater production. A reverse osmosis unit as a desalination system and a vapor compression cycle for cooling generation were utilized. Using 3E

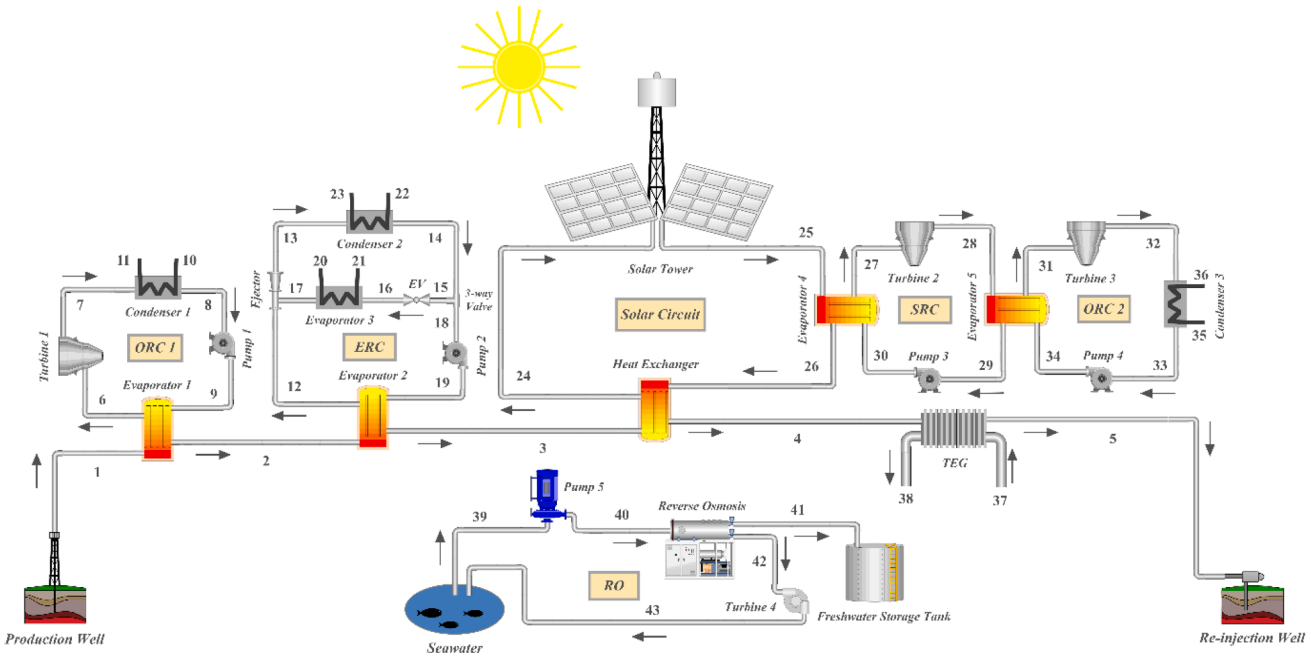

Fig. 1. A schematic of the proposed multigeneration system.

Table 1
The governing equations for the ejector section [37].

Parameter	Equation
Primary flow velocity after nozzle (m/s)	$V_{po} = \sqrt{2(h_{p,i} - h_{p,o})}$
Actual Velocity in the mixing chamber (m/s)	$V_m = V_{po} \times \frac{\sqrt{\eta_m}}{1+\mu}$
Specific enthalpy of the mixed flow (kJ/kg)	$h_m = \frac{h_{p,i} + \mu h_{s,o}}{1+\mu} - \frac{{V_m}^2}{2}$
Specific enthalpy at diffuser outlet (kJ/kg)	$h_{d,o} = h_m + \frac{{V_m}^2}{2}$
Actual specific enthalpy at diffuser outlet (kJ/kg)	$h_{d,o,ac} = \frac{h_{d,o,is} - h_m}{\eta_d} + h_m$
Entrainment ratio	$\mu = \frac{\dot{m}_s}{\dot{m}_p} = \sqrt{\eta_n \eta_m \eta_d (\frac{h_{p,i} - h_{p,o,is}}{h_{d,o,is} - h_m})}$

Table 2
The governing equations for TEG section [39].

Parameter	Equation
Mean temperature (°C)	$T_m = \frac{T_c + T_h}{2}$
Carnot efficiency	$\eta_{Carnot} = 1 - \frac{T_c}{T_h}$
TEG efficiency	$\eta_{TEG} = \eta_{Carnot} \frac{\sqrt{1+ZT_m} - 1}{\sqrt{1+ZT_m} + \frac{T_c}{T_h}}$
Generated power	$\dot{W}_{TEG} = \eta_{TEG} \dot{Q}_C$
Energy balance	$\dot{Q}_h = \dot{Q}_C + \dot{W}_{TEG}$

methods and performing multi-objective optimization, they showed that their system could reach 29.15% exergy efficiency, 1.5 $/GJ total cost per exergy unit, and 81.57 kg/s potable water production. In another study, Li et al. (2022) [18] devised a five-stage system to maximize heat recovery from a flash-binary geothermal system. A humidification-dehumidification desalination unit and an ejector refrigeration cycle were employed along with other subsystems. The multi-objective optimization was conducted based on thermodynamic and economic approaches and the results showed that the system could achieve 46.44% exergy efficiency, 3.98 $/GJ total unit cost of products, and 0.286 kg/s

Table 3
Energy balance and exergy destruction rate equations.

Component	Energy	Exergy destruction
Evaporator 1	$\dot{m}_1 h_1 + \dot{m}_9 h_9 = \dot{m}_2 h_2 + \dot{m}_6 h_6$	$\dot{E}x_D = \dot{E}x_1 + \dot{E}x_9 - \dot{E}x_2 - \dot{E}x_6$
Turbine 1	$\dot{m}_6 h_6 = \dot{m}_7 h_7 + \dot{W}_{T1}$	$\dot{E}x_D = \dot{E}x_6 - \dot{E}x_7 - \dot{W}_{T1}$
Condenser 1	$\dot{m}_7 h_7 + \dot{m}_{10} h_{10} = \dot{m}_8 h_8 + \dot{m}_{11} h_{11}$	$\dot{E}x_D = \dot{E}x_7 + \dot{E}x_{10} - \dot{E}x_8 - \dot{E}x_{11}$
Pump 1	$\dot{m}_8 h_8 + \dot{W}_{P1} = \dot{m}_9 h_9$	$\dot{E}x_D = \dot{E}x_8 - \dot{E}x_9 + \dot{W}_{P1}$
Evaporator 2	$\dot{m}_2 h_2 + \dot{m}_{19} h_{19} = \dot{m}_{12} h_{12} + \dot{m}_3 h_3$	$\dot{E}x_D = \dot{E}x_2 + \dot{E}x_{19} - \dot{E}x_2 - \dot{E}x_6$
Ejector Section	$\dot{m}_{12} h_{12} + \dot{m}_{17} h_{17} = \dot{m}_{13} h_{13}$	$\dot{E}x_D = \dot{E}x_{12} + \dot{E}x_{17} - \dot{E}x_{13}$
Condenser 2	$\dot{m}_{13} h_{13} + \dot{m}_{22} h_{22} = \dot{m}_{14} h_{14} + \dot{m}_{23} h_{23}$	$\dot{E}x_D = \dot{E}x_{13} + \dot{E}x_{22} - \dot{E}x_{14} - \dot{E}x_{23}$
Three-way valve	$\dot{m}_{14} h_{14} = \dot{m}_{15} h_{15} + \dot{m}_{18} h_{18}$	$\dot{E}x_D = \dot{E}x_{14} - \dot{E}x_{15} - \dot{E}x_{18}$
Pump 2	$\dot{m}_{18} h_{18} + \dot{W}_{P2} = \dot{m}_{19} h_{19}$	$\dot{E}x_D = \dot{E}x_{18} - \dot{E}x_{19} + \dot{W}_{P2}$
Expansion valve	$h_{15} = h_{16}$	$\dot{E}x_D = \dot{E}x_{15} - \dot{E}x_{16}$
Evaporator 3	$\dot{m}_{16} h_{16} + \dot{m}_{21} h_{21} = \dot{m}_{17} h_{17} + \dot{m}_{20} h_{20}$	$\dot{E}x_D = \dot{E}x_{16} + \dot{E}x_{21} - \dot{E}x_{17} - \dot{E}x_{20}$
Heat Exchanger	$\dot{m}_3 h_3 + \dot{m}_{26} h_{26} = \dot{m}_4 h_4 + \dot{m}_{24} h_{24}$	$\dot{E}x_D = \dot{E}x_3 + \dot{E}x_{26} - \dot{E}x_4 - \dot{E}x_{24}$
Heliostat	$\dot{m}_{24} h_{24} = \dot{m}_{25} h_{25}$	$\dot{E}x_D = \dot{E}x_{24} + \dot{E}x_{solar} - \dot{E}x_{25}$
Evaporator 4	$\dot{m}_{25} h_{25} + \dot{m}_{30} h_{30} = \dot{m}_{26} h_{26} + \dot{m}_{27} h_{27}$	$\dot{E}x_D = \dot{E}x_{30} + \dot{E}x_{25} - \dot{E}x_{26} - \dot{E}x_{27}$
Turbine 2	$\dot{m}_{27} h_{27} = \dot{m}_{28} h_{28} + \dot{W}_{T2}$	$\dot{E}x_D = \dot{E}x_{27} - \dot{E}x_{28} - \dot{W}_{T2}$
Pump 3	$\dot{m}_{29} h_{29} + \dot{W}_{P3} = \dot{m}_{30} h_{30}$	$\dot{E}x_D = \dot{E}x_{29} - \dot{E}x_{30} + \dot{W}_{P3}$
Evaporator 5	$\dot{m}_{28} h_{28} + \dot{m}_{34} h_{34} = \dot{m}_{29} h_{29} + \dot{m}_{31} h_{31}$	$\dot{E}x_D = \dot{E}x_{28} + \dot{E}x_{34} - \dot{E}x_{29} - \dot{E}x_{31}$
Turbine 3	$\dot{m}_{31} h_{31} = \dot{m}_{32} h_{32} + \dot{W}_{T3}$	$\dot{E}x_D = \dot{E}x_{31} - \dot{E}x_{32} - \dot{W}_{T3}$
Condenser 3	$\dot{m}_{32} h_{32} + \dot{m}_{35} h_{35} = \dot{m}_{33} h_{33} + \dot{m}_{36} h_{36}$	$\dot{E}x_D = \dot{E}x_{32} + \dot{E}x_{35} - \dot{E}x_{36} - \dot{E}x_{33}$
Pump 4	$\dot{m}_{33} h_{33} + \dot{W}_{P4} = \dot{m}_{34} h_{34}$	$\dot{E}x_D = \dot{E}x_{33} - \dot{E}x_{34} + \dot{W}_{P4}$
TEG	$\dot{m}_4 h_4 + \dot{m}_{37} h_{37} = \dot{m}_5 h_5 + \dot{m}_{38} h_{38} + \dot{W}_{TEG}$	$\dot{E}x_D = \dot{E}x_4 + \dot{E}x_{37} - \dot{E}x_5 - \dot{E}x_{38} + \dot{W}_{TEG}$
HP pump	$\dot{m}_{39} h_{39} + \dot{W}_{P5} = \dot{m}_{40} h_{40}$	$\dot{E}x_D = \dot{E}x_{39} - \dot{E}x_{40} + \dot{W}_{P5}$
RO unit	$\dot{m}_{40} h_{40} = \dot{m}_{41} h_{41} + \dot{m}_{42} h_{42}$	$\dot{E}x_D = \dot{E}x_{40} - \dot{E}x_{41} - \dot{E}x_{42}$
Pelton turbine	$\dot{m}_{42} h_{42} = \dot{m}_{43} h_{43} + \dot{W}_{T4}$	$\dot{E}x_D = \dot{E}x_{42} - \dot{E}x_{43} - \dot{W}_{T4}$

Table 4
The capital cost of each component.

Component	Capital cost ($)
Heat Exchangers (ORC and ejector) [22]	$Z_{HX1} = 130\left(\frac{A}{0.093}\right)^{0.78}$
ORC and SRC turbines [46]	$Z_{tur,R} = 3880\dot{W}_{tur,R}^{0.70} \times \left(1+\left(\frac{0.05}{1-\eta_{tur,R}}\right)^{3}\right) \times \left(1+5\exp\left(\frac{T^{*}-866}{10.42}\right)\right)$
Ejector Pump [22]	$Z_{pump,eje} = 3540\dot{W}_{pump,eje}^{0.71}$
ORC pumps [22]	$Z_{pump,ORC} = 2100\left(\frac{\dot{W}_{pump,ORC}}{10}\right)^{0.26} \times \left(\frac{1-\eta_{pump,ORC}}{\eta_{pump,ORC}}\right)^{0.5}$
SRC pump [46]	$Z_{pump,SRC} = 705.48\dot{W}_{pump,SRC}^{0.71} \times (1+\frac{0.2}{1-\eta_{pump,SRC}})$
SRC heat exchangers (evaporator and condenser) [46]	$Z_{HX2} = 280.74\frac{\dot{Q}}{2200\times LMTD} + 746\dot{m}$
Heliostat [20]	$Z_{hel} = 150A_hN_h$
Ejector	$Z_{eje} = 0$
Expansion Valve	$Z_{exp} = 0$
TEG [22]	$Z_{TEG} = 1500\dot{W}_{TEG}$
RO unit [17]	$Z_{RO} = C_k \times n_e \times n_v + C_{pv} \times n_v + 996(24M_f)^{0.8} + Z_{pump6} + Z_{tur,RO}$
	$Z_{pump6} = \begin{cases} 52(M_f\Delta P/100) & M_f \le 200 \\ 81(M_f\Delta P/100)^{0.96} & M_f > 200 \end{cases}$
	$Z_{tur,RO} = 2.25 + 1.497\log_{10}(\dot{W}_{T4}) - 0.1618(\log_{10}(\dot{W}_{T4}))^2$

*All temperatures are in Kelvin.

Table 5
Exergoeconomic balance and auxiliary relations.

Component	Balance relations	Auxiliary relations
Geothermal well	–	$c_1 = 1.5\$/GJ$ [22]
ORC 1 Evaporator	$\dot{C}_2 + \dot{C}_6 = \dot{C}_1 + \dot{C}_9 + \dot{Z}_{HX1}$	$c_1 = c_2$
Ejector Evaporator	$\dot{C}_3 + \dot{C}_{12} = \dot{C}_2 + \dot{C}_{19} + \dot{Z}_{HX1}$	$c_2 = c_3$
Geothermal heat exchanger	$\dot{C}_4 + \dot{C}_{24} = \dot{C}_3 + \dot{C}_{26} + \dot{Z}_{HX1}$	$c_{26} = c_{24}$
TEG	$\dot{C}_5 + \dot{C}_{38} + \dot{C}_{46} = \dot{C}_4 + \dot{C}_{37} + \dot{Z}_{TEG}$	$c_4 = c_5, c_{37} = c_{41}\&c_{46} = c_{50}$
ORC 1 turbine	$\dot{C}_7 + \dot{C}_{47} = \dot{C}_6 + \dot{Z}_{tur,R}$	$c_6 = c_7$
ORC 1 condenser	$\dot{C}_{11} + \dot{C}_8 = \dot{C}_7 + \dot{C}_{10} + \dot{Z}_{HX1}$	$c_7 = c_8\&c_{10} = 0$
ORC 1 pump	$\dot{C}_9 = \dot{C}_{47} + \dot{C}_8 + \dot{Z}_{pump,ORC}$	$c_{47} = c_{48}$
Ejector	$\dot{C}_{13} = \dot{C}_{12} + \dot{C}_{17} + \dot{Z}_{eje}$	–
Ejector condenser	$\dot{C}_{14} + \dot{C}_{23} = \dot{C}_{13} + \dot{C}_{22} + \dot{Z}_{HX1}$	$c_{13} = c_{14}\&c_{22} = 0$
Ejector three-way valve	$\dot{C}_{15} + \dot{C}_{18} = \dot{C}_{14}$	$c_{15} = c_{18}$
Ejector pump	$\dot{C}_{19} = \dot{C}_{18} + \dot{C}_{49} + \dot{Z}_{pump,eje}$	$c_{47} = c_{49}$
Ejector expansion valve	$\dot{C}_{16} = \dot{C}_{15} + \dot{Z}_{exp}$	–
Ejector evaporator	$\dot{C}_{17} + \dot{C}_{21} = \dot{C}_{16} + \dot{C}_{20} + \dot{Z}_{HX1}$	$c_{16} = c_{17}\&c_{21} = c_{41}$
Heliostat	$\dot{C}_{25} = \dot{C}_{24} + \dot{Z}_{hel}$	–
SRC evaporator	$\dot{C}_{26} + \dot{C}_{27} = \dot{C}_{25} + \dot{C}_{30} + \dot{Z}_{HX2}$	$c_{25} = c_{26}$
SRC turbine	$\dot{C}_{28} + \dot{C}_{50} = \dot{C}_{27} + \dot{Z}_{tur,R}$	$c_{27} = c_{28}$
SRC pump	$\dot{C}_{30} = \dot{C}_{29} + \dot{C}_{51} + \dot{Z}_{pump,SRC}$	$c_{51} = c_{47}$
SRC condenser/ ORC 2 evaporator	$\dot{C}_{29} + \dot{C}_{31} = \dot{C}_{28} + \dot{C}_{34} + \dot{Z}_{HX1}$	$c_{28} = c_{29}$
ORC 2 pump	$\dot{C}_{34} = \dot{C}_{33} + \dot{C}_{52} + \dot{Z}_{pump,ORC}$	$c_{47} = c_{52}$
ORC 2 turbine	$\dot{C}_{32} + \dot{C}_{53} = \dot{C}_{31} + \dot{Z}_{tur,R}$	$c_{31} = c_{32}\&c_{50} = c_{53}$
ORC 2 condenser	$\dot{C}_{33} + \dot{C}_{36} = \dot{C}_{32} + \dot{C}_{35} + \dot{Z}_{HX1}$	$c_{32} = c_{33}\&c_{35} = 0$
RO unit	$\dot{C}_{41} + \dot{C}_{42} = \dot{C}_{39} + \dot{C}_{54} + \dot{Z}_{RO}$	$c_{39} = 0\& \; c_{54} = c_{46} + c_{50} + c_{53}$ $\&c_{41} = c_{42}$
RO turbine	$\dot{C}_{45} + \dot{C}_{55} = \dot{C}_{44} + \dot{Z}_{tur,RO}$	$c_{44} = c_{45}\&c_{55} = c_{47}$

Table 6
Overall heat transfer coefficients where heat exchange occurs.

Component	U(kW/m^2-K)
Geothermal heat exchanger	1
Evaporators	1.6
Condensers	1
Ejector Evaporator	0.9

freshwater.

Solar energy, similarly, has been employed in multiple studies on multigeneration systems as the primary energy source. Yilmaz (2018) [19] used a solar tower coupled with a gas turbine to drive a multigeneration system. A flash desalination unit and an absorption cooling cycle were also utilized. Based on the thermodynamic analysis, energy efficiency, exergy efficiency, and freshwater production rate were obtained as 78.93%, 47.56%, and 0.8862 kg/s, respectively. Adding a high-temperature phase change material, Abbasi and Pourrahmani (2020) [20] modified the same upper cycle used in the study of Yilmaz (2018) to keep their trigeneration system working 24/7. They also used a reverse osmosis (RO) unit and an absorption refrigeration system. The results revealed that, at the optimal condition, the system accomplished 40.52% energy efficiency, 14.40% exergy efficiency, 30.5 $/GJ total cost of products, and 5209.5 m^3/day freshwater production.

Utilizing dual sources of renewables for driving energy systems has been considered a reliable means of providing stable supply, especially when one of the two is of intermittent nature, such as solar and wind energy. Of hybrid energy sources, geothermal and solar are most commonly investigated thus far. As a result, a fair number of studies can be found that assessed multigeneration systems utilizing these two energy sources simultaneously. Javadi et al. (2021) [21] studied a geothermal- and solar-based multigeneration system using a solar tower, an alkaline electrolyzer, and a single-stage absorption cycle for heating, cooling, electricity, and hydrogen production. They applied the energy, exergy, and exergoeconomic methods. It was found that energy efficiency and exergy efficiency were 19% and 19.29%, respectively. Employing the same methodology and producing the same products, Mahmoudan et al. (2022) [22] proposed, analyzed, and optimized a novel system utilizing parabolic trough collectors to absorb solar irradiation. The results showed that the system could acquire 35.2% exergy efficiency and 37.8 $/GJ total unit cost of products at its optimum condition.

Researchers may also furnish multigeneration systems driven by geothermal and solar energy with desalination units, enabling them to produce freshwater in areas with prevalent water scarcity. By integrating a bifacial PV plant with a geothermal heat source, Temiz and Dincer (2020) [23] proposed an energy system for heating, electricity, hydrogen, and freshwater production. Energy efficiency, exergy efficiency, and freshwater production rate were calculated to be 16%, 15%, and 14551 kg/day, respectively. It was also shown that the system posed a 4.29% internal rate of return. Siddiqui and Dincer (2020) [24] presented a system entailing a geothermal line, a solar tower, an absorption cooling system, a reverse osmosis unit, and an ammonia fuel cell subsystem for generating cooling, electricity, hydrogen, and freshwater. Energy and exergy methods were applied to analyze the system but no

economic approach and optimization was considered. The proposed system achieved 42.3% energy efficiency, 21.3% exergy efficiency, and an 87.3 kg/s freshwater production rate. This has been thus far the only study on multigeneration systems using a geothermal heat source and a solar tower for freshaterwater production.

For further clarification, the details of the abovementioned papers are also listed in the following table:

In the present study, a novel multigeneration system driven by geothermal and solar thermal energy is proposed. The arrangement includes two major interconnected parts constituting night and day modes, repsectively: geothermally-driven for electricity and cooling load generation, and solar-driven for producing heating load, electricity, and freshwater. The main purpose of this investigation is to devise an efficient and cost-effective multigeneration system primarily for fresh-

The details of the systems and the results of the studies mentioned in the introduction section.

Reference	Energy source(s)	Solar system	Products	Exergy Efficiency (%)	Total unit cost of products ($/GJ)	Water production (kg/s)
Koc et al. (2022) [12]		Not used		25.39	–	–
Akrami et al. (2017) [13]		Not used		49.17	22.73	–
Mahmoudan et al. (2021) [17]		Not used		29.15	1.5	81.57
Li et al. (2022) [18]		Not used		46.44	3.98	0.286
Islam et al. (2018) [25]				51.7	–	–
Yilmaz (2018) [19]				47.56	–	0.886
Abbasi and Pourrahmani (2020) [20]				14.4	30.5	60.3
Mahmoudan et al. (2022) [22]				35.2	37.8	–
Javadi et al. (2021) [21]				19.29	–	–
Temiz and Dincer (2020) [23]				15	–	0.168
Siddiqui and Dincer (2020) [24]				21.3	–	87.3

Heating load | Cooling load | Electricity | Hydrogen | Freshwater

Solar energy | Geothermal energy | Parabolic trough collectors | Solar tower

Table 7
Comparing the results obtained for the simulation of the ejector refrigeration unit with that of Wang et al. [37].

State	T (°C)		h (kJ/kg)		s (kJ/kg•K)		$\dot{E}x$(kW)	
	Present study	Wang (2019)	Present study	Wang (2019)	Present study	Wang (2019)	Present study	Wang (2019)
14*	35.55	35.56	285.4	286.1	1.287	1.289	5.461	5.457
15	80	80	661.6	662.3	2.382	2.384	11.993	11.99
16	50.96	50.82	631.4	632	2.412	2.414	12.58	12.6
17	35	35	283.7	284.3	1.286	1.288	9.015	9.033
18	35	35	283.7	284.3	1.286	1.288	5.287	5.283
19	35	35	283.7	284.3	1.286	1.288	3.728	3.751
20	10	10	283.7	284.3	1.297	1.299	3.471	3.49
21	10	10	567.8	568.4	2.300	2.302	2.633	2.647
22	25.53	25.53	588.8	589.4	2.311	2.313	4.126	4.149

* The same numbering as in [37].

Table 8
A validation of the reverse osmosis unit according to the results of [41].

Variable	Unit	Present study	Nafey and Sharaf (2010)
M_f	m^3/h	488.7	485.9
M_b	m^3/h	342.1	340.1
SR	–	0.9944	0.9944
X_b	ppm	64,177	64,180
X_d	ppm	252	252
ΔP	kPa	6872	6850
HPP Power	kW	1131	1131

water production. Regarding the relevant literature, the only similar study in terms of configuration and the main output (freshwater) is the one investigated in [24]. Nevertheless, that study conducted merely a thermodynamic evaluation and did not take into account any economic assessments or optimization. Therefore, the novelty of the current study is to bridge this gap by incorporating an exergoeconomic analysis and performing multi-objective optimization to yield a broader insight into such a layout. In the following, more details of the current investigation's contribution are outlined:

- Presenting a unique arrangement of a self-sustained system using geothermal and solar thermal energy for heating load, cooling load, electricity, and freshwater production.
- Employing thermodynamic and economic methods (i.e., energy, exergy, and exergoeconomics) to evaluate system performance and measure the size of outputs through a parametric study.
- Performing multi-objective optimization for maximizing exergy efficiency and minimizing the total cost of products to detect optimal decision variables.
- Presenting in-depth visualization of the cost flow balance within the system for a better comparison of input/output costs.
- Carrying out a case study based on optimal decision variables to examine system performance and evaluate the freshwater production rate in a seaside, arid region.

Table 9
Input parameters for the base case study.

Parameter	Unit	Value
Ambient temperature	°C	25
Ambient pressure	kPa	101.32
Pinch point temperature difference	°C	10
Geothermal unit		
Working fluid	–	Water
Temperature	°C	150
Pressure	kPa	800
Mass flow rate	kg/s	10
Organic Rankine cycle [47]		
Working fluid of ORC 1	–	Isobutane
Working fluid of ORC 2	–	Toluene
Turbine isentropic efficiency	%	80
Pump isentropic efficiency	%	85
Condenser temperature of ORC 1	°C	30
Condenser temperature of ORC 2	°C	35
Ejector refrigeration cycle [37]		
Working fluid	–	Isobutane
Main pressure	kPa	1250
Condenser temperature	°C	35
Evaporator Temperature	°C	0
Pump isentropic efficiency	%	85
Nozzle efficiency	%	85
Mixing efficiency	%	90
Diffuser efficiency	%	85
Solar circuit		
Direct normal irradiation	W/m^2	600
Number of heliostats	–	50
Heliostat width	m	10
Heliostat height	m	10
Receiver efficiency	%	88
Optical efficiency	%	75
Mass flow rate inside the circuit	kg/s	5
Pressure inside the circuit	kPa	180
Working fluid	–	Air
TEG [22]		
The figure of merit	–	1
Cold end temperature difference	°C	5
Domestic hot water unit		
Temperature	°C	70
Steam Rankine Cycle		
High pressure	kPa	3000
Low pressure	kPa	80
Turbine isentropic efficiency	%	90
Pump isentropic efficiency	%	85
Reverse osmosis unit [17]		
Recovery ratio	–	0.3
Salt rejection percentage	%	99.44
The salinity of seawater	ppm	35
Fouling factor	–	0.85
Element Area	m^2	35.4
Number of elements	–	7
Number of pressure vessels	–	42
High-pressure pump efficiency	%	80
Specific heat of seawater	kJ/kg-k	3.85
Price of pressure vessel	$	7000
Price of each membrane	$	1200
Pelton turbine isentropic efficiency	%	90

2. System description

From the configuration depicted in Fig. 1, we can see that the system contains various components, through which different commodities are generated. By extracting heat from an injection well via geothermal water, the system provides permanently accessible green energy. At state 1, the geothermal hot water goes through the evaporator of the first organic Rankine cycle (ORC1), where heat is transferred to Isobutane (the working fluid of ORC1). The power generated in this subsystem will be sent to the grid after supplying the electricity required for all pumps except for that of a desalination unit. An ejector refrigeration unit consumes the remaining geothermal heat to generate cooling load for residential buildings. This part of the system operates with no interruption throughout the entire day.

The diurnal section of the system is driven by solar energy, which is provided by a solar tower. The intense heat produced by the heliostat field is mostly removed by a steam Rankine cycle (SRC), which is also connected to an organic Rankine cycle (ORC2). All the power generated by these two subsystems is transferred to the pump of a reverse osmosis (RO) unit. Before closing the solar circuit, the remaining heat from the working fluid heats up the geothermal line through a heat exchanger. Prior to entering the re-injection well, the geothermal line passes through a thermoelectric generator (TEG), which cogenerates electricity and hot water (state 38) simultaneously. The power provided by the TEG is also sent to the RO unit. Finally, the desalination system produces freshwater for the consumption of households. Additionally, the high-pressure brine water, rejected by the RO unit, runs a Pelton turbine to generate more electricity for the grid.

Table 10
An outline of energy, exergy, and exergoeconomic analyses for the base case study.

Parameter	Unit	Value
Exergy efficiency	%	17.2
Net output power	kW	311.4
Turbine 1 generated power	kW	262.1
Turbine 2 generated power	kW	185.7
Turbine 3 generated power	kW	48.6
Turbine 4 generated power	kW	95.8
TEG generated power	kW	7.5
Freshwater production	kg/s	15
Domestic hot water heating load	MW	1.5
Cooling load	kW	82.8
The total unit cost of products	$/GJ	59.7

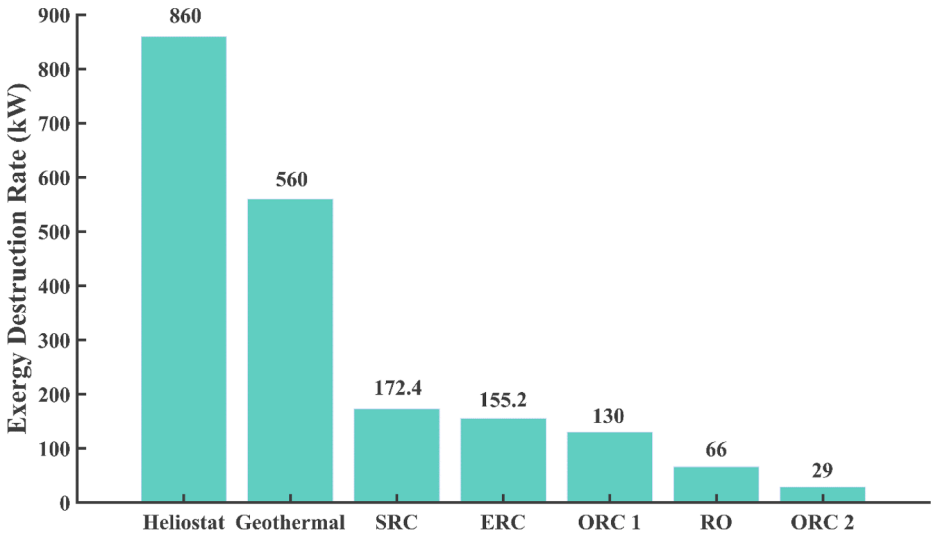

Fig. 2. Exergy destruction rate of all subsystems.

3. Thermodynamic analysis

In this study, for mass and energy equations applied to each component, the following assumptions are made [26–28]:

- Steady-state condition throughout the entire system.
- Negligible potential and kinetic energy.
- Minor pressure loss in pipes.
- Isentropic efficiency for turbines and pumps are 0.85 and 0.80, respectively.
- Saturated vapor after evaporators.
- Saturated liquid after condensers.

For each component, by considering a control volume, the governing equations can be written as follows [29,30]:

$$\sum \dot{m}_i = \sum \dot{m}_e \tag{1}$$

$$\sum \dot{m}_i h_i + \dot{Q} = \sum \dot{m}_e h_e + \dot{W} \tag{2}$$

Where i and o denote inlet and outlet, respectively.

A Matlab code, with the use of Refprop 9 software, which provides thermodynamic properties of working fluids, is developed to simulate the proposed system in this study. The properties of seawater, however, were obtained according to [31,32].

In the following, the thermodynamic model of each subsystem is given:

3.1. Ejector

An ejector is a suction chamber that mixes two incoming streams in a constant pressure environment. A blend of a high-pressure flow (primary flow) and a low-pressure flow (secondary flow) takes place in this component in order to convert kinetic energy into pressure head through a constant-area section [33]. In this regard, the ratio of the secondary mass flow rate to that of the primary flow is called the entrainment ratio of an ejector:

$$\mu = \frac{\dot{m}_s}{\dot{m}_p} \tag{3}$$

Subscript s and p stand for secondary and primary flows in the ejector section, respectively [34–36]. Other equations associated with the ejector simulation are tabulated in Table 1.

3.2. Thermoelectric generator (TEG)

In addition to electricity, a thermoelectric generator produces hot water for domestic use as a waste heat recovery unit. The Seebeck effect occurs in thermoelectric generators (TEG) to convert heat into electricity [38]. The performance of TEG is directly related to the figure of merit (z_{TM}), a parameter that represents the internal conversion efficiency. The governing equations for the TEG unit are listed in Table 2.

3.3. Solar tower

The heat exchange between the working fluid in the heliostat and solar receivers can be written as:

$$\dot{m}_{24} h_{24} + \dot{Q}_{rec} = \dot{m}_{25} h_{25} \tag{4}$$

In which, $\dot{Q}_{rec}$is the solar thermal energy rate received by a solar tower that depends on direct normal irradiation (DNI), surface area of each heliostat (A_h), number of heliostats (N), optical (η_{opt}) and receiver (η_{rec}) efficiencies according to equation (5):

$$\dot{Q}_{rec} = \eta_{opt} \eta_{rec} N A_h DNI \tag{5}$$

Depending on the geographical location of a heliostat field, DNI takes a distinct value for each hour of day within a year, A_h is the multiply of the length and width of a heliostat, and η_{opt} and η_{rec} are considered constant in this study [40].

3.4. Reverse osmosis

Reverse osmosis (RO), a power-driven water-treatment system, is one of the prevalent means for desalinating seawater. In this section, the mathematical model of an RO unit is developed:

The recovery ratio is defined as the ratio of distillate mass flow rate to the seawater feed flow rate [41]:

$$RR = \frac{\dot{m}_{41}}{\dot{m}_{40}} \tag{6}$$

Hence, the mass flow rate of brine water can be obtained as:

$$\dot{m}_{42} = \dot{m}_{40} - \dot{m}_{41} \tag{7}$$

With X_f as the salt concentration of feed water, the corresponding parameter for distilled water is obtained as:

$$X_d = X_f (1 - SR) \tag{8}$$

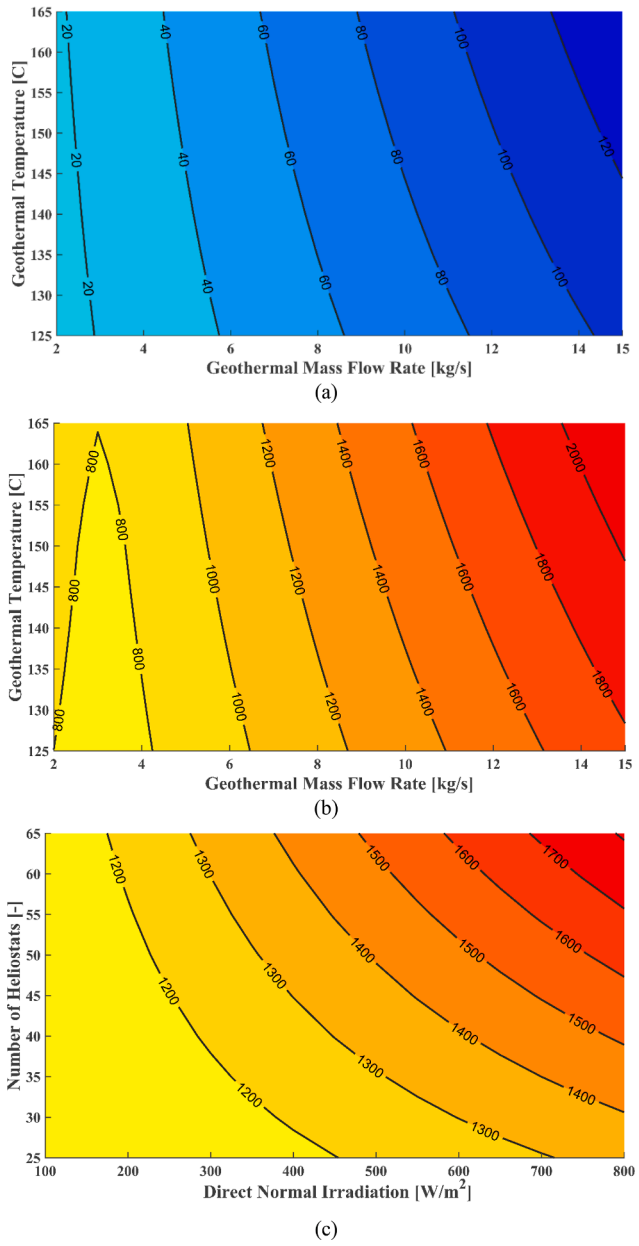

Fig. 3. Contours for the impact of geothermal decision variables, i.e., temperature and mass flow rate, on (a) cooling load and (b) heating load, and solar decision variables, i.e., number of heliostats and DNI, on (c) heating load.

Here, *SR* is the salt rejection percentage.

Having these two concentrations, the feed flow salinity can be calculated as follows:

$$X_b = \frac{X_f - RRX_d}{1 - RR} \tag{9}$$

The temperature correction factor is defined as:

$$TCF = \exp(2700 \times (\frac{1}{T_k} - \frac{1}{298}) \tag{10}$$

Water permeability for the membrane is given as:

$$k_w = \frac{6.84 \times 10^{-8} \times (18.6865 - (0.177 \times X_d))}{T_k} \tag{11}$$

For osmosis pressure average and net values, we have:

$$P_{av} = 37.92 \times (X_f + X_b) \tag{12}$$

$$P_{net} = P_{av} - 75.84 \times X_d \tag{13}$$

Pressure difference through the membrane is:

$$\Delta P = \frac{\dot{m}_{39}}{3600 \times TCF \times FF \times A_e \times n_e \times n_v \times k_w} + P_{net} \tag{14}$$

Finally, the power required for high-pressure pump can be formulated as below:

$$\dot{W}_{HP} = \frac{100 \times \dot{m}_{39} \times \Delta P}{3600 \times \rho_f \times \eta_p} \tag{15}$$

4. Exergy analysis

In addition to the energy analysis presented in the previous section, using the exergy method, which is adapted from the second thermodynamic law, could be worthwhile. This is characterized by the amount of available energy for producing useful work. Adopting this approach will also enable us to quantify exergy destruction rates in all components [42]. The general form of the exergy balance relation can be formulated as below:

$$\sum \dot{m}_{in} ex_{in} + \dot{E}x_Q = \sum \dot{m}_{out} ex_{out} + \dot{E}x_W + \dot{E}x_D \tag{16}$$

Where $\dot{E}x_Q$, $\dot{E}x_W$, and $\dot{E}x_D$ represent exergy rates of heat transfer and work and exergy destruction rate, respectively. By considering a reference state for measuring the maximum accessible work, the specific exergy can be given as [43]:

$$ex = (h - h^0) - T_0(s - s^0) + \sum x_i ex_{ch} + T_0 \sum x_i R_i ln y_i \tag{17}$$

The specific exergy consists of physical, chemical, kinetic, and potential terms. Also, "0" denotes the dead state condition, in which $T_0 =$ 298 K and $P_0 = 101.325$ kPa. In equation (17), x_i and y_i are mass and mole fractions, respectively.

The exergy of solar radiation can be defined by equation (18). In this equation, T_{amb} is the ambient temperature and T_{sun} is the temperature of the sun, which is 5770 K [44].

$$\dot{E}x_{solar} = \dot{Q}_r(1 - \frac{4}{3}\left(\frac{T_{amb}}{T_{sun}}\right) + \frac{1}{3}\left(\frac{T_{amb}}{T_{sun}}\right)^4) \tag{18}$$

For all system components, energy and exergy balance equations can be found in Table 3.

5. Exergoeconomic analysis

The Exergoeconomic method, which is a combination of thermodynamic and economic approaches, is used in this study to assess the system from the economic perspective. In this regard, the governing exergoeconomic balance equation for each component can be written as follows:

$$\dot{C}_{Q,k} + \sum_i \dot{C}_{i,k} + \dot{Z}_k = \dot{C}_{w,k} + \sum_e \dot{C}_{e,k} \tag{19}$$

$$\dot{C}_j = c_j \dot{E}x_j \tag{20}$$

Where $\dot{C}$ is the cost rate related to flow exergy, c denotes cost rates per exergy unit, and subscripts Q and W refer to heat transfer and work, respectively. $\dot{Z}$ that denotes the cost rate of each component is calculated as a levelized parameter by the below equation [45]:

$$\dot{Z}_k = \frac{CRF \times Z \times N}{3600} \tag{21}$$

$$CRF = \frac{i(1+i)^n}{(1+i)^n - 1} \tag{22}$$

Here, *CRF* is the capital recovery factor, and *Z* is the total cost ($) of

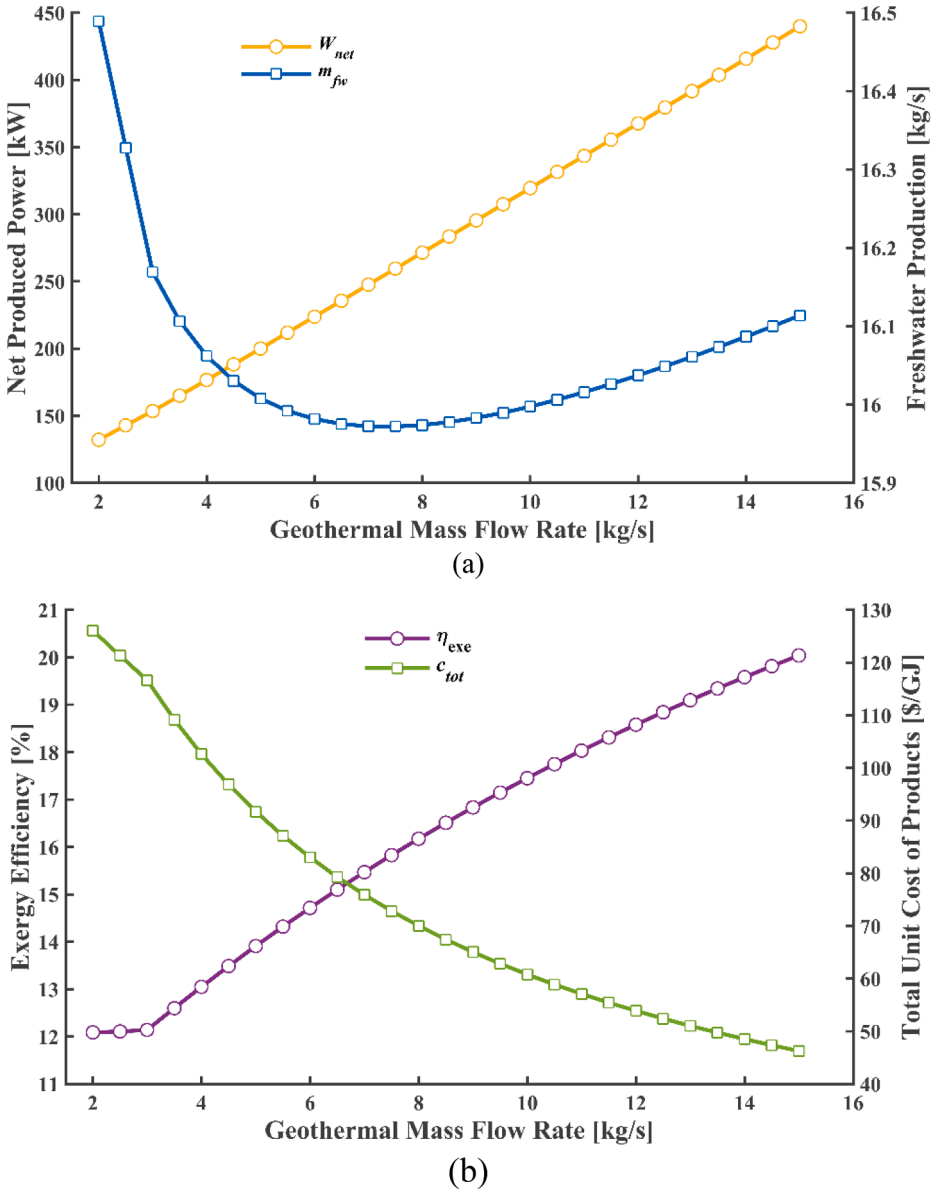

Fig. 4. Impact of geothermal mass flow rate on (a) net produced power and freshwater production and (b) exergy efficiency and total unit cost of products.

each component, defined individually in Table 4. Moreover, N, i, and n are the total operating time (8000 h), the interest rate (12%), and system lifetime (20 years), respectively.

By implementing Eq. (19), the equations listed in Table 5 can be generated for each component. The combination of these equations generates a system of exergoeconomic relations with the cost rates per exergy unit as unknowns, which are as large as 55 for the proposed system. To solve it, a companion of auxiliary relations is also necessary to close the given system of equations and reach a unique solution. Moreover, the corresponding total heat transfer coefficient is needed to calculate heat transfer in heat exchangers, as given in Table 6.

At the end of this section, the proposed system's performance indicators are defined as below:

$$\eta_{exe} = \frac{\dot{W}_{net} + \dot{E}x_{21} + \dot{E}x_{38} + \dot{E}x_{41}}{\dot{E}x_1 + \dot{E}x_{solar}} \tag{23}$$

Here, η_{exe} is total exergy efficiency of the system, and $\dot{W}_{net}$ is the net output power defined as:

$$\dot{W}_{net} = \dot{W}_{T1} + \dot{W}_{T4} - (\dot{W}_{P1} + \dot{W}_{P2} + \dot{W}_{P3} + \dot{W}_{P4}) \tag{24}$$

To evaluate the economic performance of the system, the total unit cost of products may be used, as defined below:

$$c_{tot} = \frac{\dot{C}_{Wnet} + \dot{C}_{21} + \dot{C}_{38} + \dot{C}_{41}}{\dot{W}_{net} + \dot{E}x_{21} + \dot{E}x_{38} + \dot{E}x_{41}} \tag{25}$$

Where $\dot{C}_{Wnet}$ is the cost of net output power ($).

6. Model validation

Since no exact arrangement can be found in the literature, the proposed system cannot be validated altogether. Therefore, validation must be done subsystem-wise. There are two complex units for validation: ejector refrigeration and reverse osmosis. The validation of the former is presented in Table 7. Comparing the results of the four evaluated parameters with that of [37] shows that the level of accuracy in our simulation is at an acceptable level. Moreover, the result obtained for the reverse osmosis unit has been compared with that of [41] to make a validation case. As can be seen in Table 8, there is a negligible discrepancy between the two outcomes.

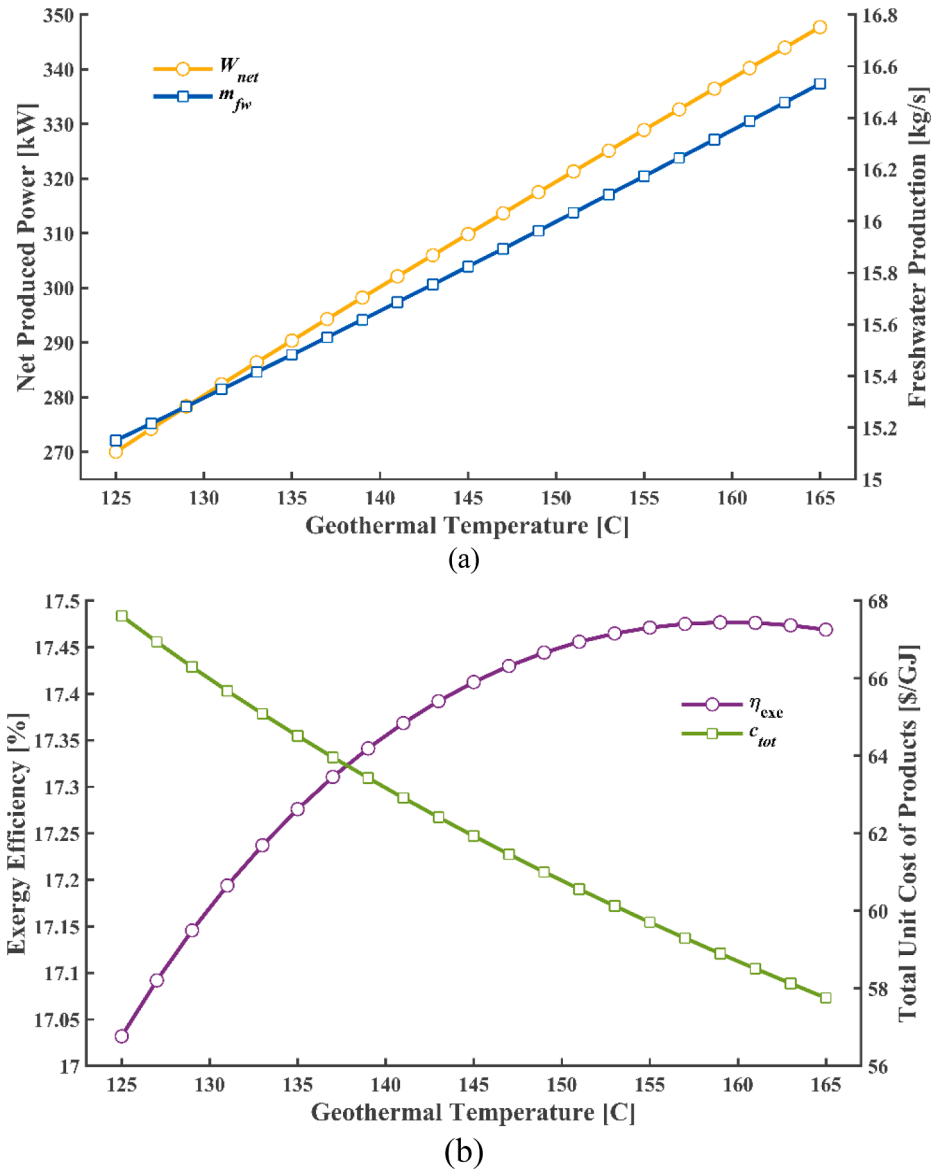

Fig. 5. Impact of geothermal temperature on (a) net produced power and freshwater production and (b) exergy efficiency and total unit cost of products.

7. Results and discussion

The input data used in the simulation of a base case study is given in Table 9. The results obtained for this simulation are also tabulated in Table 10. The power sent to the RO unit is a combination of produced electricity by turbine 2, turbine 3, and TEG which makes an aggregate of 241.8 kW. This amount of power produces 15 kg/s freshwater in the RO subsystem. The power sent to the grid is generated through turbine 1 and turbine 4 minus the power required by other pumps in the system. There is 357.9 kW total electricity generated by those two turbines, while the net output power is 311.4 kW, meaning that 46.5 kW power is consumed by all pumps except for the RO pump. Moreover, the system exhibits a total exergy efficiency of 17.2%, and a total unit cost of products of 59.7 $/GJ. The relatively low value of exergy efficiency can be ascribed to high exergy destruction in the solar tower. Finally, the cooling and heating loads are calculated to be 82.8 kW and 1.5 MW, respectively.

Note that the base case study provides a ground for comparison with the outcome of the multi-objective optimization that will be presented in section 7.2. It will be shown that how much improvement, regarding exergy efficiency and the total unit cost of products, would be attained when employing optimal decision variables.

The exergy destruction of each subsystem is shown in Fig. 2. Obviously, the solar tower exerts the highest rate of exergy destruction, with 860 kW. This is the main reason for the low value of total exergy efficiency. The second highest exergy destruction rate (560 kW) occurs in the geothermal line, which is comprised of three heat exchangers and a TEG unit. Other subsystems cause fewer than 200 kW exergy destruction rate, ranging from 172.4 kW to 29 kW, in the following order: SRC, ERC, ORC 1, RO, and ORC 2. Heat exchangers mainly cause a relatively higher exergy destruction effect, especially when the incoming heat is great. Also, the number of heat exchangers in a unit may have a direct relationship with the amount of exergy destruction rate caused by that unit. In this regard, the geothermal line includes three heat exchangers, SRC has two, ERC has three (but at lower temperatures compared to SRC), and each of ORC 1 and ORC 2 has two.

7.1. Parametric study

In this section, the impact of the main decision variables (i.e., geothermal mass flow rate, geothermal temperature, number of heliostats, and DNI) on performance indicators is evaluated. In Fig. 3a-b, the

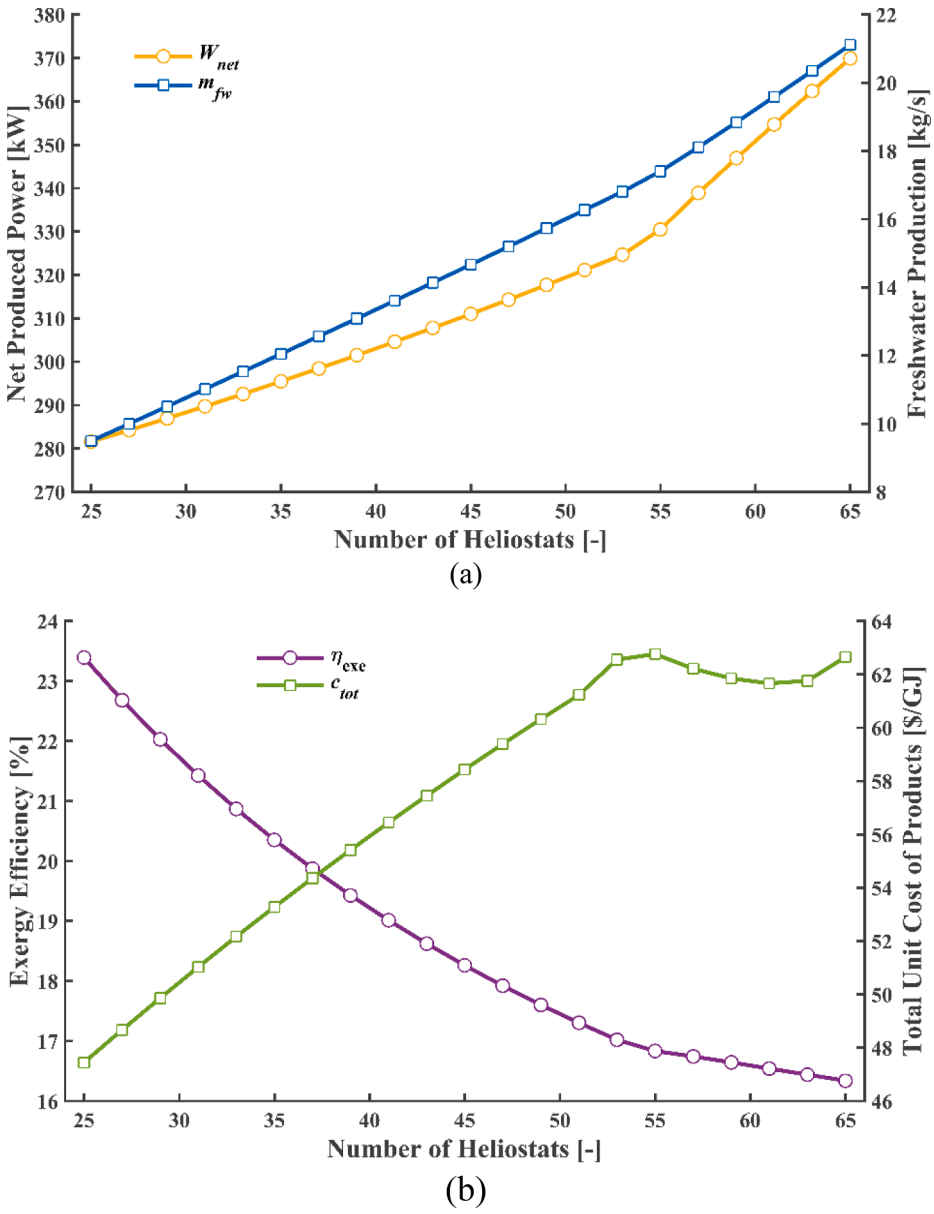

Fig. 6. Impact of the number of heliostats on (a) net produced power and freshwater production and (b) exergy efficiency and total unit cost of products.

Table 11
The range of decision variables considered for the multi-objective optimization process.

Parameter	Range
Geothermal mass flow rate, $\dot{m}_{geo}$ (kg/s)	2–15
Geothermal temperature, T_{geo} (℃)	125–165
Number of heliostat, N (–)	25–65
The pressure of Rankine cycle, P_{HRank} (kPa)	2000–5000
The figure of merit, Z_{TM} (–)	0.2–2

Table 12
Control parameters of the optimization process.

Parameter	Value
Population size	90
Maximum generations	250
Crossover probability	0.8
Mutation probability	0.05
Selection process	Tournament

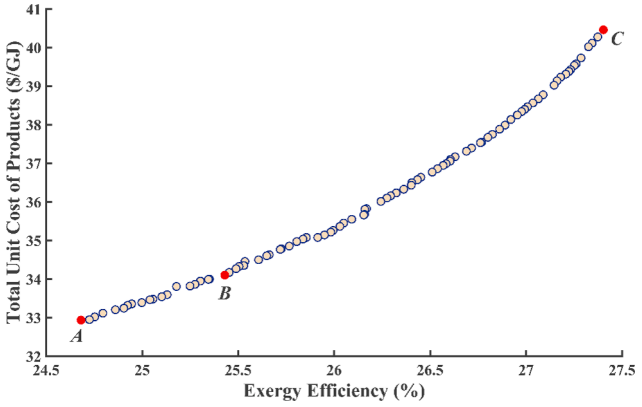

Fig. 7. The Pareto frontier obtained from the multi-objective optimization.

Table 13
The corresponding input values and results of the points *A*, *B*, and *C* on the Pareto frontier.

Variable	*A*	*B*	*C*
T_{geo}(°C)	125.1	154	165
$\dot{m}_{geo}$ (kg/s)	15	15	15
N(–)	25	25	25
P_{SRC}(kPa)	4689.5	3125.1	3423
ZT_m(–)	0.68	0.21	0.20
η_{exe}(%)	27.4	25.4	24.7
$\dot{m}_{fw}$(kg/s)	7.3	9.1	9.4
$\dot{W}_{net}$(kW)	331.4	423.7	453.3
c_{tot}($/GJ)	40.5	34.1	32.9

change of cooling and heating loads based on simultaneous alteration of the two geothermal decision variables (i.e., geothermal mass flow rate and geothermal temperature) are shown. The result of a similar analysis for the solar circuit's decision variables (i.e., number of heliostats and DNI) can also be observed in Fig. 3c. As depicted in Fig. 3a, the geothermal mass flow rate has a greater effect than the geothermal temperature on the cooling load, which varies from 20 kW to 130 kW. Changing geothermal decision variables also changes domestic hot water production (Fig. 3b). Again, the mass flow rate plays a more dominant role in heating load generation. Finally, from Fig. 3c, it can be inferred that both the number of heliostats and DNI have somewhat similar effects on domestic hot water production.

The effect of the first three decision variables on performance indicators is addressed in the following. These performance indicators are exergy efficiency, the total unit cost of products, net produced power, and freshwater production. Regarding Fig. 4, as the geothermal mass flow rate changes from 2 to 15, net produced electricity escalates by more than double, while the freshwater mass flow rate declines by merely 2%. Since the power for the RO unit is supplied by three power-generating units (i.e., SRC, ORC 2, and TEG), a complex relationship exists between the geothermal mass flow rate and the produced freshwater mass flow rate, as shown in Fig. 4a. At 2 kg/s, the TEG produces a relatively high amount of power, but this value declines at higher geothermal mass flow rates. On the other hand, SRC and ORC 2 produce more power at higher geothermal mass flow rates, pushing the freshwater production curve a little bit higher. Regarding Fig. 4b, it is evident that high geothermal mass flow rates can improve exergy efficiency and decrease total cost. At 15 kg/s, both performance indicators are improved by nearly 65% compared to the results of the lowest geothermal mass flow rate. This indicates that the system performs better at higher geothermal mass flow rates and it can be validated after carrying out optimization.

In comparison with the geothermal mass flow rate, the geothermal temperature demonstrates a less significant effect on all output variables (Fig. 5). As the geothermal water temperature rises from 125 °C to 165 °C, there is almost 8% enhancement of freshwater production, 14%

Table 14
Thermodynamic and exergoeconomic results at all state points at the optimum performance.

State Point	Fluid	m(kg/s)	T(°C)	P(kPa)	h(kJ/kg)	s(kJ/kg•K)	$\dot{E}x$(kW)	c($/GJ)	$\dot{C}$($/h)
1	Water	15	154	800	649.5	1.9	1400	1.50	7.5
2	Water	15	107.8	800	452.5	1.4	622.9	1.50	3.4
3	Water	15	75.4	800	316.5	1.1	251.4	1.50	1.4
4	Water	15	84.2	800	353.2	1.1	336.9	3.9	4.8
5	Water	15	54.7	800	229.7	0.8	97.6	3.9	1.4
6	Isobutane	5.9	143.9	2500	778.2	2.6	884.2	2.4	7.8
7	Isobutane	5.9	89.8	404.7	709.6	2.7	397.2	2.4	3.5
8	Isobutane	5.9	30	404.7	271.2	1.3	295.6	2.4	2.6
9	Isobutane	5.9	31.4	2500	275.8	1.3	318.2	2.8	3.2
10	Seawater	12.9	25	101.3	99.8	0.4	0	0	0
11	Seawater	12.9	74.8	101.3	299.5	0.9	193.8	3.2	2.2
12	Isobutane	4.9	97.8	1250	702.5	2.5	533.3	4.2	8.1
13	Isobutane	5.4	80.6	464.8	689.5	2.6	373.5	6.2	8.3
14	Isobutane	5.4	35	464.8	283.7	1.3	271.7	6.2	6.0
15	Isobutane	0.5	35	464.8	283.7	1.3	23.8	6.2	0.5
16	Isobutane	0.5	0	156.9	283.7	1.3	20.9	7.0	0.5
17	Isobutane	0.5	0	156.9	554.3	2.3	9.3	7.0	0.2
18	Isobutane	4.9	35	464.8	283.7	1.3	247.8	6.2	5.5
19	Isobutane	4.9	35.5	1250	285.4	1.3	255.1	6.5	6.0
20	Water	1.5	25	101.3	104.9	0.4	0	0	0
21	Water	1.5	5	101.3	21.1	0.1	4.5	24.8	0.4
22	Seawater	13.4	25	101.3	99.8	0.4	0	0	0
23	Seawater	13.4	65.6	101.3	262.6	0.9	135.7	6.5	3.2
24	Air	5	90.4	180	488.2	3.9	277.5	5.9	5.9
25	Air	5	283.7	180	686.2	4.3	617.1	5.9	13.1
26	Air	5	198.6	180	598.2	4.2	432.9	5.9	9.2
27	Water	0.2	273.7	3125	2920	6.4	177.5	6.4	4.1
28	Water	0.2	93.5	80	2347	6.6	68.6	6.4	1.6
29	Water	0.2	93.5	80	391.7	1.2	4.9	6.4	0.1
30	Water	0.2	93.8	3125	395.4	1.2	5.6	7.6	0.2
31	Toluene	3.9	83.5	2500	−51.2	−0.2	47.6	10.9	1.9
32	Toluene	3.9	35	6.2	−58.7	−0.2	11.2	10.9	0.4
33	Toluene	3.9	35	6.2	−141.1	−0.4	0.7	10.9	0.1
34	Toluene	3.9	35.9	2500	−137.6	−0.4	12.3	8.1	0.4
35	Seawater	16.3	25	101.3	99.8	0.4	0	0	0
36	Seawater	16.3	30	101.3	119.7	0.4	2.3	86.4	0.4
37	Water	9.8	25	101.3	104.9	0.4	0	0	0
38	Water	9.8	70	101.3	292.9	0.9	126.5	6.8	3.1
39	Seawater	30.9	25	101.3	99.8	0.4	0	0	0
40	Seawater	30.9	25	3761.2	103.1	0.3	110.3	103.5	41.1
41	Freshwater	9.1	25	180	104.9	0.4	50.7	137.6	25.1
42	Brine	21.8	25	2820.9	99.9	0.3	57.4	137.6	28.4
43	Brine	21.8	25	101.3	97.5	0.3	0	137.6	0

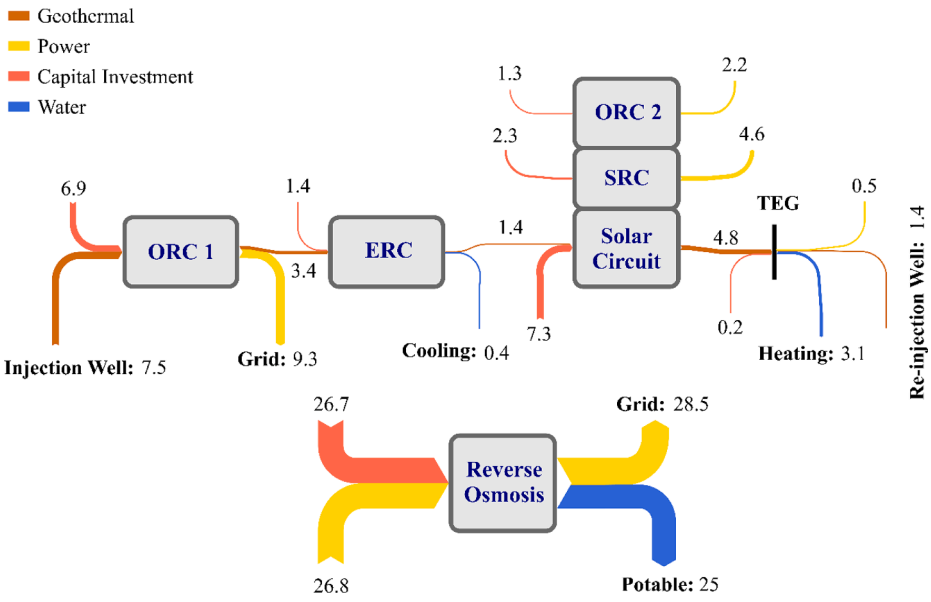

Fig. 8. Sankey diagram depicting cost flow rates of the proposed system ($/h).

Table 15
Geographical and meteorological data of Minab.

Item	Value
Latitude	27.15°
Longitude	57°
Elevation	40 m
Relative humidity (summer at 12:00)	40 %
Dry bulb temperature	42.5 ℃

lower cost rate, 2.5% exergy efficiency improvement, and 30% net produced electricity boost. As one can notice, total exergy efficiency reaches its peak at a geothermal temperature value of around 154 °C, implying to be potentially an optimal value. It is clear that overall system performance is also enhanced in this case.

As shown in Fig. 6a, the number of heliostats can have a far-reaching effect on freshwater production, causing an almost 110% growth. Net produced electricity also sees a 90 kW improvement as the number of heliostats increases from 25 to 65. On the other hand, Fig. 6b shows that the total exergetic performance of the system declines and the total unit cost of products increases, with 30% and 32%, respectively. It suggests a low number of heliostats as a sensible decision. This is in harmony with the main objective of the optimization process we aim to carry out in the next section that means to regulate decision variables to attain maximum exergy efficiency while keeping the total cost of products as low as possible.

In summary, among the three decision variables studied parametrically, the geothermal mass flow rate exhibited the greatest impact; all performance indicators were altered significantly except for freshwater production. It is followed by the number of heliostats, the impact of which moderately changed all the investigated outputs. Finally, the geothermal temperature demonstrated a comparably negligible effect on all performance indexes except for net produced power.

7.2. Multi-objective optimization

Regulating energy systems to simultaneously have minimal total cost and excellent performance requires finding proper values for decision variables. This can only be fulfilled by performing multi-objective optimization based on the two aforementioned criteria. The NSGA-II

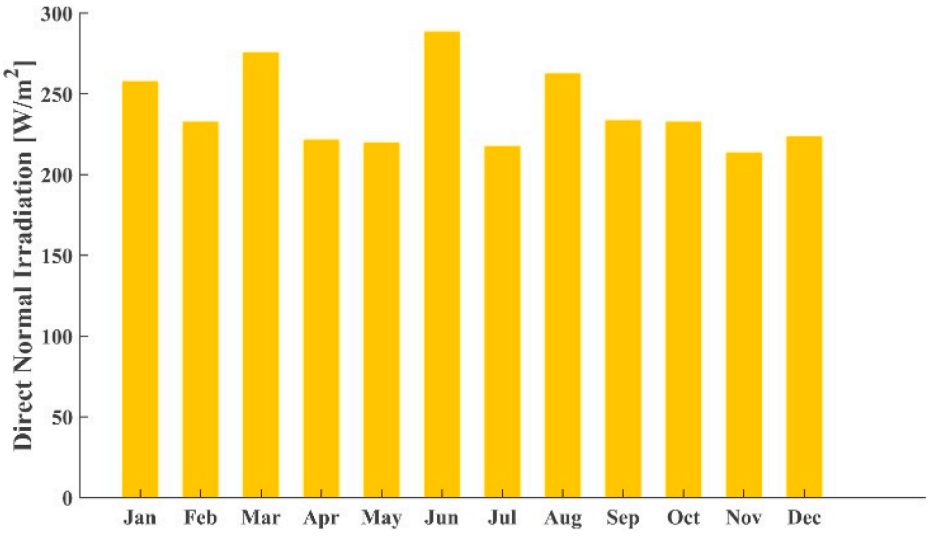

Fig. 9. Average DNI of each month in Minab.

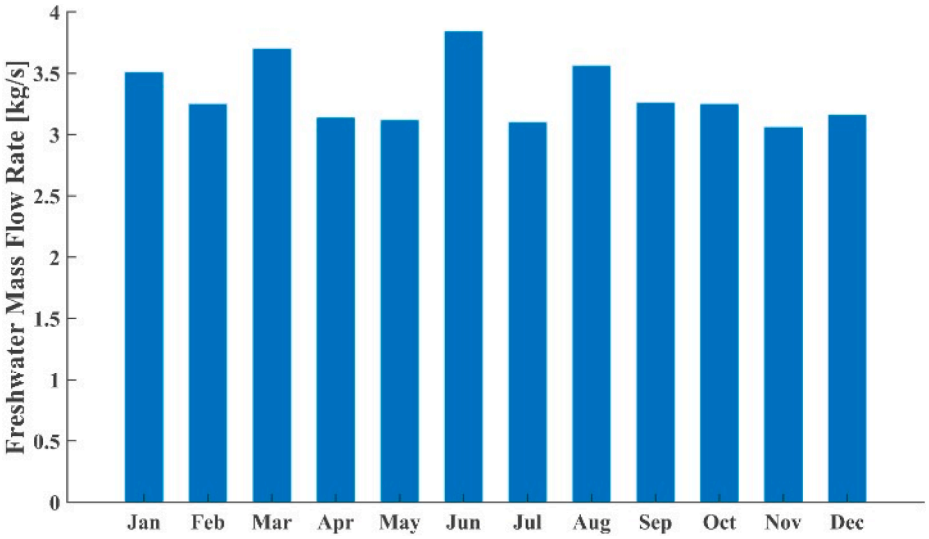

Fig. 10. Variation of freshwater mass flow rate produced by the system in different months in Minab.

Table 16
The amount of performance indicators and the population coverage of produced freshwater when the system operates in Minab.

Month	η_{exe}(%)	c_{tot}($/GJ)	$\dot{W}_{net}$(kW)	$\dot{m}_{fw}$(kg/s)	Population coverage of freshwater (individual)
January	31.2	28.8	374.5	3.51	1404
February	31.7	28.7	373.1	3.25	1300
March	30.9	28.9	375.5	3.70	1480
April	32.0	28.7	372.5	3.14	1256
May	32.1	28.7	372.4	3.12	1248
June	30.6	28.9	376.2	3.84	1536
July	32.1	28.7	372.3	3.10	1240
August	31.1	28.8	374.7	3.56	1424
September	31.7	28.7	373.2	3.26	1304
October	31.7	28.7	373.1	3.25	1300
November	32.1	28.7	372.1	3.06	1224
December	31.9	28.7	372.6	3.16	1264

algorithm [48] is implemented in this study to carry out multi-objective optimization where the objective functions are overall exergy efficiency and the total unit cost of products. To make sure that the final results are achieved with reasonable accuracy, the number of generations and population size were set as 250 and 90, respectively. The ranges of five decision variables used for this aim are given in Table 11. The pressure of Rankine cycle and the figure of merit are also included as they have significant effect on freshwater production. Moreover, the control parameters opted for the optimization process are given in Table 12.

The results of the optimization process, the Pareto frontier, are depicted in Fig. 7. In order to select the best solution out of all points, the TOPSIS method is employed. Giving an identical weight to each objective function, point B is found to be the finest trade-off solution. Also, A and C are the best points in terms of the total cost rate and exergy efficiency, respectively. The decision variables and the corresponding results of these three points are tabulated in Table 13. Therefore, when operated optimally, the system presents 25.4% exergy efficiency and 34.1 $/GJ total unit cost of products. Compared to the outcome of the base case study given in Table 10, in which exergy efficiency was reported as 17.2% and the total unit cost of products was 59.7 $/GJ, the improvements at optimal performance are approximately 48% and 43%, respectively. To provide more details, the thermodynamic and exergoeconomic properties of all state points are given in Table 14.

7.3. System cost flows

At the optimal condition, the major cost flow rates of the system are graphically illustrated in Fig. 8 via a Sankey diagram. As can be seen, the cost rate of the incoming geothermal heat is 7.5 $/h which decreases stage by stage up until the solar circuit. In the first subsystem (ORC 1), the cost rate of power generation for the grid is 9.3 $/h. Regarding the cost balance in this unit, the remaining cost rate (1.7 $/h) is related to pump 1 and the 11th stream. In ERC, generating cooling load costs 0.4 $/h, and the extra 3 $/h can be attributed to pump 2 and the 23rd stream. Since the solar circuit, SRC, and ORC 2 are connected in a cascade way, they can be taken as a compact unit for the sake of simplicity. From the cost balance in this unit, the remaining cost rate (0.7 $/h) relates to the contribution of pump 3, pump 4, and the 36th stream. The power output of this block of units is 6.8 $/h. After receiving heat from the solar circuit, the cost rate of the geothermal line at state 4 rises to 4.8 $/h. This stream goes into the TEG unit, in which electricity and hot water are produced at 0.5 $/h and 3.1 $/h, respectively. As can be observed from the RO unit, it possesses the highest capital cost rate in the entire system, with 26.7 $/h. This subsystem also produces the costliest products; freshwater, at 25 $/h, and electricity, at 28.5 $/h. Overall, electricity, with 37.8 $/h, makes the most expensive product followed by freshwater.

7.4. Case study

As the optimal decision variables of the proposed system were identified previously, it is of practical value to examine the system in a case study while operating at its optimum condition. For this purpose, Minab city in Hormozgan province, Iran is chosen since it suffers from water scarcity. This dry spot is situated near the Persian Gulf, enjoys abundant solar energy throughout the year, and is potentially a good location for geothermal energy extraction. Based on these characteristics, Minab makes a suitable place for testing renewable energy penetration. Table 15 lists the basic data for this city. The average direct normal irradiation of Minab in different months is depicted in Fig. 9. As observed, June and November, with 289 W/m^2 and 214 W/m^2, have the highest and lowest DNIs, respectively. The system's freshwater production rate is also exhibited in Fig. 10 which its pattern is fairly similar to that of the DNI. Table 16 lists the average values of exergy efficiency, total unit cost of products, electricity generation, and freshwater production rate monthly. Compared to the optimization results presented in Table 13, exergy efficiency and total unit cost of products take more

desirable values in this case study. This may be due to the lower values of DNI compared to 600 W/m^2 considered in the optimization process. This demonstrates that the system operates more efficiently at lower DNIs. Note that the variation of the total unit cost of products throughout the year is somewhat negligible. The reason is that the quantity of this parameter largely depends on the net produced electricity, the monthly variation of which is similarly marginal. Table 16 also indicates the number of individuals receiving freshwater based on the average value of water consumption per person, which is 220 L per day (≅ 0.0025 kg/s) [49]. The number of people who can benefit from the produced potable water ranges from 1224 to 1536 in a year for Minab.

8. Conclusion

In this study, an innovative multigeneration system utilizing renewable energy sources (i.e., geothermal and solar) for producing heating load, cooling load, electricity, and freshwater has been proposed. Energy, exergy, and exergoeconomic analyses were applied to examine the system from diverse standpoints. The effect of decision variables on overall performance was scrutinized through parametric study, and multi-objective optimization was conducted to discover their optimal values. Based on these values, a case study was conducted to evaluate system performance under the meteorological condition of Minab city on a monthly basis. The following notes can be concluded from this study:

- Regarding the base case study, the following results were obtained: 17.2% total exergy efficiency, 59.7 $/GJ total cost rate of products, 15 kg/s potable water production, 82.8 kW cooling load, 1.5 MW heating load, and 311.4 kW generated electricity for the grid.
- Exergy destruction results showed that the solar tower and the geothermal line had the highest exergy destruction rates, at 860 kW and 560 kW, respectively.
- Among the three decision variables examined via parametric study, the geothermal mass flow rate, number of heliostats, and geothermal temperature had successively the highest to the least impact on the performance indicators.
- Five decision variables were opted to perform multi-objective optimization, for which exergy efficiency and total unit cost of products were selected as objective functions. At the optimum condition, exergy efficiency, freshwater mass flow rate, electricity generation, and total unit cost of products were 25.4%, 9.1 kg/s, 423.7 kW, and 34.1 $/GJ, respectively.
- Using the DNI of Minab and employing the optimal inputs, the monthly performance of the system was evaluated for this region. The results exhibited that the highest attainable freshwater rate was 3.84 kg/s, providing drinkable water for as many as 1536 individuals.

Declaration of Competing Interest

The authors declare that they have no known competing financial interests or personal relationships that could have appeared to influence the work reported in this paper.

Data availability

Data will be made available on request.

References

[1] H.O. Pörtner, D.C. Roberts, H. Adams, C. Adler, P. Aldunce, E. Ali, R.A. Begum, R. Betts, R.B. Kerr, R. Biesbroek, J. Birkmann. Climate change 2022: impacts, adaptation and vulnerability, IPCC, Geneva, Switzerland, 2022.

[2] L. Stougie, N. Giustozzi, H. van der Kooi, A. Stoppato, Environmental, economic and exergetic sustainability assessment of power generation from fossil and renewable energy sources, Int. J. Energy Res. 42 (2018) 2916–2926.

[3] A. Farahmand-Zahed, S. Nojavan, K. Zare, B. Mohammadi-Ivatloo, Economic and Environmental Benefits of Renewable Energy Sources in Multi-generation Systems, Integr Clean Sustain Energy Resour Storage Multi-Generation Syst (2020) 1–14, https://doi.org/10.1007/978-3-030-42420-6_1.

[4] P. Nojedehi, M. Heidari, A. Ataei, M. Nedaei, E. Kurdestani, Environmental assessment of energy production from landfill gas plants by using Long-range Energy Alternative Planning (LEAP) and IPCC methane estimation methods: A case study of Tehran, Sustain Energy Technol Assessments 16 (2016) 33–42.

[5] I. Dincer, C. Zamfirescu, Renewable-energy-based multigeneration systems, Int. J. Energy Res. 36 (2012) 1403–1415, https://doi.org/10.1002/ER.2882.

[6] K. Li, H. Bian, C. Liu, D. Zhang, Y. Yang, Comparison of geothermal with solar and wind power generation systems, Renew. Sustain. Energy Rev. 42 (2015) 1464–1474.

[7] United Nations Development Programme. World energy assessment: Energy and the challenge of sustainability. UNDP, 2000.

[8] M.H. Dickson, M. Fanelli, Geothermal energy: Utilization and technology, 1st ed. Taylor and Francis, London, 2013. https://doi.org/10.4324/9781315065786.

[9] P.L. Younger, Geothermal energy: delivering on the global potential, Energies 8 (2015) 11737–11754.

[10] D. Millstein, P. Dobson, S. Jeong, The potential to improve the value of US geothermal electricity generation through flexible operations, J. Energy Res. Technol. (2021) 143.

[11] K. Hansen, B.V. Mathiesen, Comprehensive assessment of the role and potential for solar thermal in future energy systems, Sol. Energy 169 (2018) 144–152.

[12] M. Koc, Y.E. Yuksel, M. Ozturk, Thermodynamic and exergo-economic assessments of a new geothermally driven multigeneration plant, Int. J. Hydrogen Energy (2022).

[13] E. Akrami, A. Chitsaz, H. Nami, S.M.S. Mahmoudi, Energetic and exergoeconomic assessment of a multi-generation energy system based on indirect use of geothermal energy, Energy 124 (2017) 625–639.

[14] N. Azizi, F. Esmaeilion, S.F. Moosavian, M. Yaghoubirad, A. Ahmadi, M. Aliehyaei, et al., Critical review of multigeneration system powered by geothermal energy resource from the energy, exergy, and economic point of views, Energy Sci. Eng. 10 (2022) 4859–4889.

[15] F. Yilmaz, Development and modeling of the geothermal energy based multigeneration plant for beneficial outputs: Thermo-economic and environmental analysis approach, Renew. Energy 189 (2022) 1074–1085.

[16] F. Yilmaz, M. Ozturk, R. Selbas, Modeling and design of the new combined double-flash and binary geothermal power plant for multigeneration purposes; thermodynamic analysis, Int. J. Hydrogen Energy 47 (2022) 19381–19396.

[17] A. Mahmoudan, P. Samadof, S. Hosseinzadeh, D.A. Garcia, A multigeneration cascade system using ground-source energy with cold recovery: 3E analyses and multi-objective optimization, Energy 233 (2021), 121185.

[18] K. Li, Y.-Z. Ding, C. Ai, H. Sun, Y.-P. Xu, N. Nedaei, Multi-objective optimization and multi-aspect analysis of an innovative geothermal-based multi-generation energy system for power, cooling, hydrogen, and freshwater production, Energy 245 (2022), 123198.

[19] F. Yilmaz, Thermodynamic performance evaluation of a novel solar energy based multigeneration system, Appl. Therm. Eng. 143 (2018) 429–437.

[20] H.R. Abbasi, H. Pourrahmani, Multi-objective optimization and exergoeconomic analysis of a continuous solar-driven system with PCM for power, cooling and freshwater production, Energy Convers Manag 211 (2020), 112761.

[21] M.A. Javadi, M.K. Abhari, R. Ghasemiasl, H. Ghomashi, Energy, exergy and exergy-economic analysis of a new multigeneration system based on double-flash geothermal power plant and solar power tower, Sustain Energy Technol Assessments 47 (2021), 101536.

[22] A. Mahmoudan, F. Esmaeilion, S. Hoseinzadeh, M. Soltani, P. Ahmadi, M. Rosen, A geothermal and solar-based multigeneration system integrated with a TEG unit: Development, 3E analyses, and multi-objective optimization, Appl. Energy 308 (2022), 118399.

[23] M. Temiz, I. Dincer, Techno-economic assessment of bifacial photovoltaic and geothermal based multigeneration system for cleaner communities, J. Clean. Prod. 275 (2020), 122879.

[24] O. Siddiqui, I. Dincer, A new solar and geothermal based integrated ammonia fuel cell system for multigeneration, Int. J. Hydrogen Energy 45 (2020) 34637–34653.

[25] S. Islam, I. Dincer, B.S. Yilbas, Development, analysis and assessment of solar energy-based multigeneration system with thermoelectric generator, Energy Convers Manag 156 (2018) 746–756.

[26] S. Hoseinzadeh, B. Nastasi, D. Groppi, D.A. Garcia, Exploring the penetration of renewable energy at increasing the boundaries of the urban energy system–The PRISMI plus toolkit application to Monachil, Spain. Sustain Energy Technol Assessments 54 (2022), 102908.

[27] F. Esmaeilion, M. Soltani, M.B. Dusseault, M.A. Rosen, Performance investigation of a novel polygeneration system based on liquid air energy storage, Energy Convers Manag 277 (2023), 116615.

[28] F. Esmaeilion, M. Soltani, J. Nathwani, Assessment of a novel solar-powered polygeneration system highlighting efficiency, exergy, economic and environmental factors, Desalination 540 (2022), 116004.

[29] K. Menberg, Y. Heo, W. Choi, R. Ooka, R. Choudhary, M. Shukuya, Exergy analysis of a hybrid ground-source heat pump system, Appl. Energy 204 (2017) 31–46.

[30] B.F. Tchanche, G. Lambrinos, A. Frangoudakis, G. Papadakis, Exergy analysis of micro-organic Rankine power cycles for a small scale solar driven reverse osmosis desalination system, Appl. Energy 87 (2010) 1295–1306.

[31] K.G. Nayar, M.H. Sharqawy, L.D. Banchik, V.J.H. Lienhard, Thermophysical properties of seawater: A review and new correlations that include pressure dependence, Desalination 390 (2016) 1–24, https://doi.org/10.1016/j.desal.2016.02.024.
[32] M.H. Sharqawy, J.H. Lienhard, S.M. Zubair, Thermophysical properties of seawater: a review of existing correlations and data, Desalin. Water Treat. 16 (2010) 354–380, https://doi.org/10.5004/dwt.2010.1079.
[33] B.J. Huang, J.M. Chang, C.P. Wang, V.A. Petrenko, A 1-D analysis of ejector performance, Int. J. Refrig 22 (1999) 354–364.
[34] J. Chen, H. Havtun, B. Palm, Conventional and advanced exergy analysis of an ejector refrigeration system, Appl. Energy 144 (2015) 139–151.
[35] Z. Liu, Z. Liu, X. Xin, X. Yang, Proposal and assessment of a novel carbon dioxide energy storage system with electrical thermal storage and ejector condensing cycle: Energy and exergy analysis, Appl. Energy 269 (2020), 115067.
[36] A. Mwesigye, A. Kiamari, S.B. Dworkin, Energetic optimization and exergetic performance investigation of an ejector refrigeration system using HCFO-1233zd (E) as a refrigerant, Int. J. Refrig 112 (2020) 155–171.
[37] Y. Wang, T. Chen, Y. Liang, H. Sun, Y. Zhu, A novel cooling and power cycle based on the absorption power cycle and booster-assisted ejector refrigeration cycle driven by a low-grade heat source: Energy, exergy and exergoeconomic analysis, Energy Convers Manag 204 (2020), 112321.
[38] H. Jouhara, A. Żabnieńska-Góra, N. Khordehgah, Q. Doraghi, L. Ahmad, L. Norman, et al., Thermoelectric generator (TEG) technologies and applications, Int J Thermofluids 9 (2021), 100063.
[39] C. Babu, P. Ponnambalam, The theoretical performance evaluation of hybrid PV-TEG system, Energy Convers Manag 173 (2018) 450–460.
[40] M.E. Demir, I. Dincer, Development of a hybrid solar thermal system with TEG and PEM electrolyzer for hydrogen and power production, Int. J. Hydrogen Energy 42 (2017) 30044–30056.
[41] A.S. Nafey, M.A. Sharaf, Combined solar organic Rankine cycle with reverse osmosis desalination process: Energy, exergy, and cost evaluations, Renew. Energy 35 (2010) 2571–2580, https://doi.org/10.1016/j.renene.2010.03.034.
[42] M.A. Rosen, Exergy analysis, Des. Perform. Optim. Renew. Energy Syst., Elsevier, 2021, p. 43–60.
[43] A. Bejan, G. Tsatsaronis, M.J. Moran, Thermal design and optimization, John Wiley & Sons, 1995.
[44] A. Bejan, Advanced engineering thermodynamics, John Wiley & Sons, 2016.
[45] A. Bagdanavicius, N. Jenkins, Exergy and exergoeconomic analysis of a Compressed Air Energy Storage combined with a district energy system, Energy Convers Manag 77 (2014) 432–440, https://doi.org/10.1016/j.enconman.2013.09.063.
[46] A. Mahmoudan, P. Samadof, M. Sadeghzadeh, M. Jalili, M. Sharifpur, R. Kumar, Thermodynamic and exergoeconomic analyses and performance assessment of a new configuration of a combined cooling and power generation system based on ORC–VCR, J. Therm. Anal. Calorim. 145 (2021) 1163–1189, https://doi.org/10.1007/s10973-020-10230-y.
[47] A. Mahmoudan, P. Samadof, R. Kumar, M. Jalili, A. Issakhov, Emergy-based exergoeconomic and exergoenvironmental evaluation of a combined power and cooling system based on ORC-VCR, J. Therm. Anal. Calorim. 145 (2021) 1353–1372, https://doi.org/10.1007/s10973-020-10422-6.
[48] Y. Zhou, S. Cao, R. Kosonen, M. Hamdy, Multi-objective optimisation of an interactive buildings-vehicles energy sharing network with high energy flexibility using the Pareto archive NSGA-II algorithm, Energy Convers Manag 218 (2020), 113017.
[49] A.R. Keshavarzi, M. Sharifzadeh, A.A.K. Haghighi, S. Amin, S. Keshtkar, A. Bamdad, Rural domestic water consumption behavior: A case study in Ramjerd area, Fars province, IR Iran. Water Res 40 (2006) 1173–1178.